Fizika Nizkikh Temperatur, 1997, v. 23, No 7, p. 732–737

Emission Mössbauer study of CMR manganite $La_{0.8}Ca_{0.2}MnO_3$. II. Step by step snapshots of the metal-insulator transition

Vladimir Chechersky, Kiyoshi Nomura*, and Amar Nath

Department of Chemistry, Drexel University, Philadelphia, PA 19104, U.S.A.

Honglyoul Ju** and Richard L. Greene

Center for Superconductivity Research, Department of Physics, University of Maryland, College Park, MD 20742, U.S.A.

Submitted March 21, 1997

We follow the step by step progression of events while approaching Curie temperature T_C from below using ^{57}Co substituent as microprobe in an emission Mössbauer study combined with resistivity measurements. In the temperature range $0.33 < T/T_C \le 1$, the material consists of a mixture of ferromagnetic and paramagnetic regions within the same matrix. An increase of the amount of paramagnetic fraction is accompanied by a decrease in electron delocalization in the ferromagnetic regions. At $T \ge T_C$, the electrons are localized to neighboring Mn^{4+}/Mn^{3+} pairs only, in about 46% of the paramagnetic species. The strength with which Mn atoms are bound to the neighbors also decreases progressively and rather steeply in the range $0.65 \le T/T_C = 1$. Zero field resistivity, ρ_0, follows linearly with the amount of paramagnetic phase in the range $0.65 \le T/T_C \le 1$ and still show metal-like behavior up to $T/T_C \approx 1.03$.

PACS: **76.80.+y**

Substitution of La^{3+} by Ca^{2+} converts antiferromagnetic insulator $LaMnO_3$ into the mixed valence Mn^{3+}/Mn^{4+} ferromagnetic metal which undergoes transition into the paramagnetic semiconducting state at T_C. According to the double exchange model [1], the probability of electron hopping between Mn^{3+} and Mn^{4+} via O^{2-} is controlled by relative orientation of neighboring Mn spins and is the highest when Mn ions are ordered ferromagnetically. This accounts qualitatively for the correlation between magnetic and transport properties in doped manganites. The «colossal magnetoresistance» (CMR) recently observed in this system [2–9] is the focus of considerable attention both because of the potential applications for devices and the challenge to fully understand the basic nature of the transition and the associated CMR. The several orders of magnitude decrease of resistivity in a few tesla magnetic field near T_C suggests that there is a healthy interplay between magnetic order, electronic behavior, lattice distortions, and elastic properties of the material. In a search for these correlations the simultaneous macro- and microscopic measurements performed on the same sample would be very valuable. Emission Mössbauer spectroscopy offers such a unique possibility.

Here we report the results of an emission Mössbauer effect study, where only a few tens of parts-per-million of Mn is substituted by ^{57}Co with minimal perturbation of the manganite system, in conjuction with simultaneous resistivity measurements. We follow the progressive enrichment of the

* Permanent address: Graduate School of Engineering, The University of Tokyo, Hongo 7-3-1, Bunkuo-ku, Tokyo 113.

** Present address: Lawrence Berkeley Laboratory, National Center for Electron Microscopy. Berkeley, CA 94720.

© Vladimir Chechersky, Kiyoshi Nomura, Amar Nath, Honglyoul Ju, and Richard L. Greene, 1997

ferromagnetic component in Mn^{4+} with decreasing electron delocalization as we approach the T_C from below. This is accompanied by a sharp decrease in the binding of the Mn to its neighbors. To obtain Mössbauer data, we diffused a couple of millicuries of carrier-free ^{57}Co into a compacted pellet of $La_{0.8}Ca_{0.2}MnO_3$ (sample 2, T_C = 237 K) measuring $2.5 \times 2.7 \times 12$ mm by a two step thermal treatment, viz. at 950 °C for 4–5 h followed by 6 h at 900 °C, both under O_2 flow. A gas flow cryostat was modified to allow the four probe resistivity measurements while collecting Mössbauer data.

The material was prepared by conventional solid state reaction and characterized by x-ray diffraction and magnetization measurements.

The temperature-dependent resistivity plot and Mössbauer spectra of $La_{0.8}Ca_{0.2}Mn(^{57}Co)O_3$ at corresponding temperatures are shown in Fig 1. The six line spectrum is characteristic of a magnetically ordered material while a singlet or doublet (in the case of non-zero electric field gradient on the lattice site occupied by ^{57}Co) are an indication of a paramagnetic state. We found that even at $T/T_C = 0.33$ (not shown), the sample contains only 90% of magnetic fraction, the rest is paramagnetic. The presence of only a single symmetrical sextet with relatively narrow line widths (similar to one shown in Part I of this paper for sample I Fig. 4,*b*) shows that the sample consists of a single phase, and that the microprobe, ^{57}Co, occupies the unique crystallographic site of Mn. The ferromagnetic component converts into the paramagnetic state rather gradually up to $T/T_C \approx 0.85$. Thereafter, there is a rapid increase in the concentration of the paramagnetic component till it becomes 100% at T_C = 237 K. The coexistence of ferromagnetic and paramagnetic regions within the same matrix distinguishes it from conventional ferromagnetics [10] and could be responsible for its peculiar transport and magnetic properties. For instance, a plot of the resistivity as a function of the amount of ferromagnetic fraction in the temperature range $0.65 \le T/T_C \le 1$ is linear (Fig. 2). It means that the current flows exclusively through filamentary ferromagnetic regions surrounded by paramagnetic inclusions in accord with the recently proposed model [11]. The paramagnetic phase present below T_C may be a major source of carrier scattering from $T/T_C \approx 0.6$ to T_C.

The Curie temperature as determined by the Mössbauer effect, i.e. the temperature at which the sextet collapses completely, just corresponds to the maximum of the derivative $d\rho_0/dT$. It is noteworthy that the change from metal-like conductivity to the thermally activated behavior is above the transition into the paramagnetic state by 7 K (Fig. 1). One can perhaps rationalize this observation in the following fashion. At T_C, the static magnetic order as seen by Mössbauer effect measurements vanishes. However, the temperature-dependent line shapes (i.e. broadening) of the sextet below T_C (Fig. 1) are indicative of the presence of some dynamic magnetic correlations in quasistatic magnetic regions. Correlation between these spin fluctuations could persist above T_C (with frequencies higher than about 10^{11} s^{-1}, which are above the limit of Mössbauer effect time scale) which would permit the probability of double exchange to be non-zero. This would account for the metallic behavior up to $T/T_C = 1.03$. Non-coincidence of T_C and maximum of resistivity has been reported by several researchers.

We also observe a decrease in the magnitude of the chemical shift of the ferromagnetic species as a function of temperature (Fig. 3). The chemical shift is determined by the *s*-electron density on the daughter nucleus ^{57}Fe, which in turn is determined primarily by the shielding from 3*d*-electron density — the higher the shielding the smaller will be the *s*-electron density and larger the magnitude of the chemical shift. Taking into account the expected negative thermal shift with increasing temperature due to the second order Doppler effect [12], the chemical shift (δ) for the ferromagnetic component clearly undergoes a very sharp anomalous decrease in the range $0.65 \le T/T_C = 1$ (Fig. 3). This observation is very insightful. The ferromagnetic species is progressively getting enriched in Mn^{4+} (Fe^{4+}). One can infer that the Mn^{4+} ions are sharing the delocalized electrons with less and less number of Mn^{3+} as T_C is being approached.

The paramagnetic component above T_C consists of two species (Fig. 4) with the following parameters at room temperature. Species I. $\delta = 0.44$ mm/s, Area = 54%; Species II. $\delta = 0.21$ mm/s, Area = 46%. The chemical shift for species I corresponds to daughter $^{57}Fe^{3+}$ (at Mn^{3+}) while that for species II corresponds approximately half-way between that for $^{57}Fe^{3+}$ and $^{57}Fe^{4+}$, assuming $\delta \approx 0$ for $^{57}Fe^{4+}$ at 300 K [13]. Therefore, in the paramagnetic state, 46% of material consist of Mn^{3+}/Mn^{4+} pairs with the electron shuttling between a pair, while in the remaining 54% of the material there is no delocalization of electrons and the species contains only Mn^{3+}. The observation of 46% Mn^{4+}/Mn^{3+} pairs by emission Mössbauer spectroscopy translates to the presence of 23% of Mn^{4+} because $^{57}Co(^{57}Fe)$ sitting in a Mn^{3+} site and sharing an electron with a Mn^{4+} neighbor cannot be

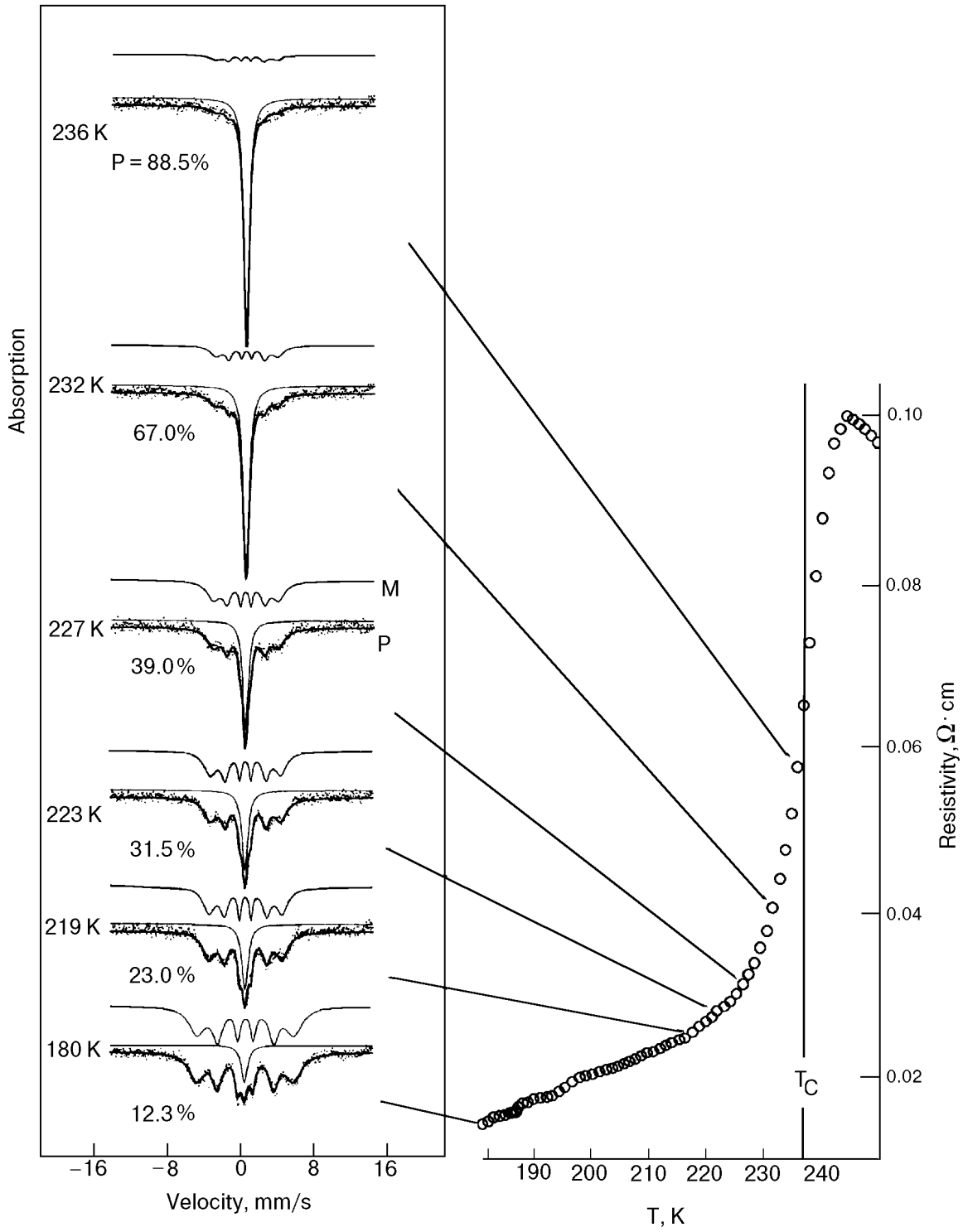

Fig. 1. The extent of ferromagnetic to paramagnetic state conversion and the change of resistivity in $La_{0.8}Ca_{0.2}Mn(^{57}Co)O_3$ as a function of temperature: P, paramagnetic component; M, ferromagnetic component . For the sake of simplicity, the two paramagnetic species (see text) have been approximated to a singlet without loss in accuracy in the computer analyses of Mössbauer spectra recorded in a wide velocity range.

distinguished from a $^{57}Co(^{57}Fe)$ situated in a Mn^{4+} site and sharing an electron with a Mn^{3+} neighbor if the exchange rate is faster than the reciprocal life time of the excited state of the Mössbauer probe (10^7 s^{-1}). This also constitutes an elegant procedure for determining the concentration of holes in manganites. Since 20% units of Mn^{4+} arise from Ca substitution, the remaining presumably arise from cation vacancies created by thermal treatment in O_2 ambient [14]. We attribute the localization of

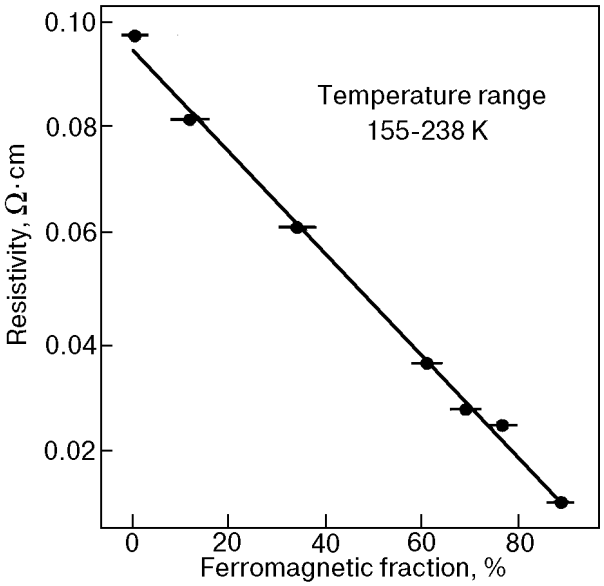

Fig. 2. A plot of resistivity versus ferromagnetic fraction in the temperature range $0.65 \le T/T_C \le 1$.

the electrons to Mn^{3+}/Mn^{4+} pairs to the distortions of the Mn–O octahedra with respect to each other introducing asymmetry. Our observations support the small polaron model [10,15–20] in the sense that the electrons are strictly localized between Mn^{4+}/Mn^{3+} pairs above T_C .

The normalized total area under the spectrum is plotted as a function of temperature in Fig 5. The

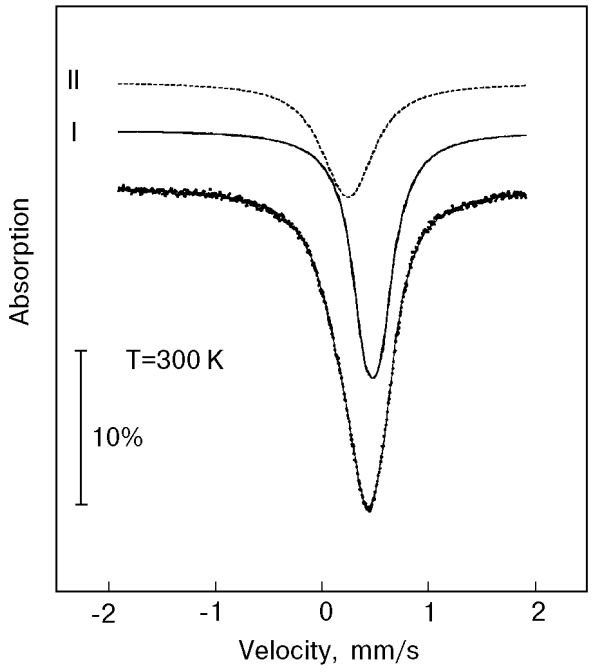

Fig. 4. Decomposition of Mössbauer spectrum of $La_{0.8}Ca_{0.2}Mn(^{57}Co)O_3$ in paramagnetic state. Species I and II correspond to two different valence states of the daughter ^{57}Fe (see text).

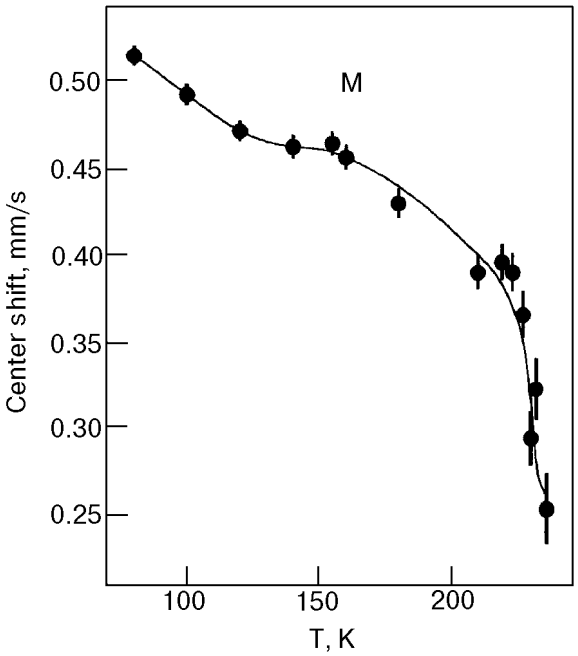

Fig. 3. A plot of the center (chemical) shift of ferromagnetic (M) species versus temperature for $La_{0.8}Ca_{0.2}Mn(^{57}Co)O_3$. The solid line is a guide for the eyes.

area of the spectrum represents the recoil-free Mössbauer events and is thus a measure of the strength with which Mn is bound to its neighbors (i.e. the Debye–Waller factor). There is a dramatic drop of the area in the range $0.65 \le T/T_C = 1$ and a minimum is attained at T_C. This clearly indicates that the amplitude of vibration for Mn is pretty large near T_C . This can again arise from torsional oscillations between Mn–O octahedra. The ferro-

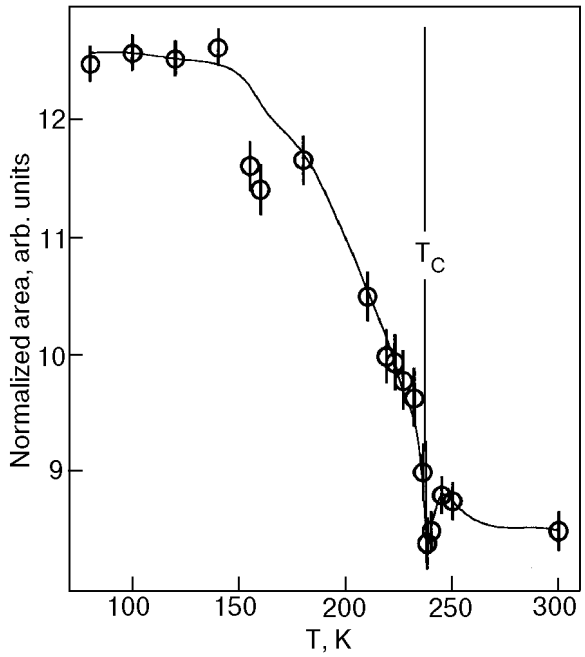

Fig. 5. A plot of normalized area under the Mössbauer spectrum as a function of temperature. The solid line is a guide for the eyes.

magnetic metal to paramagnetic insulator transition is accompanied by significant expansion ($\approx 13\%$) of the lattice [21–24]. An anomalously large amplitude of vibration for Mn (and O) atoms around T_C has been reported in [18,24,25] which was predicted earlier [20].

The conversion to the paramagnetic state, anomalous changes in chemical shift of the ferromagnetic component, and a decrease in the total area of the spectrum, take place continuously in a wide temperature range and not precipitously at a well- defined transition temperature. The decrease in density of states as determined by photoemission studies [16,26] and density of holes by Hall effect [27] for the La–Ca–Mn–O system also show a similar progressive change over a span of temperatures. Perhaps these observations are indicative of the first order transition or/and the intrinsically heterogeneous nature of the doped oxide systems (a property shared by the high temperature superconductors).

We observe almost zero quadrupole splitting for the ferromagnetic state and small values (≤ 0.15 mm/s) for the two paramagnetic species. The magnitude of quadrupole splitting depends on the degree of deviation from spherical distribution of the electron cloud (viz., electric field gradient) around ^{57}Fe nucleus. Therefore one would expect that the Mn–O bond lengths should be nearly equal in the ferromagnetic state. This rules out only the static Jahn–Teller distortions and not the dynamic ones [19,28]. On the other hand, the non-zero quadrupole splittings (about 0.15 mm/s) for both of the paramagnetic species are indicative of the fact that the Mn–O bond lengths are unequal. It is presumably due to a small Jahn–Teller distortion static or dynamic [15,18,20,29]. More importantly, the Mn–O bond lengths would differ for each of the paramagnetic species because of differing Mn valence. This is borne out by the powder neutron diffraction studies of Caignaert et al. [23] and Dai et al. [24]. They observe that the Mn–O bond lengths are nearly equal below T_C and that there is a distribution of bond lengths in the paramagnetic state. These observations are contrary to ones made by Radaelli et al. [22].

In summary, moving along the $\rho_0(T)$ plot and collecting Mössbauer spectra at specified temperatures, we obtain an insight into the microscopic nature of some transport and magnetic properties of the La–Ca–Mn–O system. The presence of paramagnetic regions far below T_C is believed to be a major source of carrier scattering from $T/T_C \approx 0.6$ to T_C . Noncoincidence of T_C and the peak of $\rho_0(T)$ is attributed to the spatial correlations of the spin fluctuations in a narrow temperature range above T_C . We also get a good measure of the different stages of the transition starting with completely delocalized electrons in the ferromagnetic phase with Mn^{3+}/Mn^{4+} ratio of about 3.5. As T approaches T_C from below, the ferromagnetic phase is continually enriched in Mn^{4+} with decreasing extent of electron delocalization. Finally, at $T \geq T_C$, the electrons are localized to neighboring Mn^{4+}/Mn^{3+} pairs only, in a considerable portion of the paramagnetic species. We also found a minimum of recoil-free fraction at T_C . The Mn atoms are undergoing larger mean square displacements in the paramagnetic phase.

Acknowledgments

A.N. thanks George McLendon for a fruitful discussion and the Donors of the Petroleum Research Fund administered by the ACS for partial support of this research. R. L. G. acknowledges support from NSF under DMR-9209668.

1. C. Zener, *Phys. Rev.* **82**, 403 (1951); P. W Anderson and H. Hasegawa, *Phys. Rev.* **100**, 675 (1955); J. B. Goodenough, *Phys. Rev.* **100**, 564 (1955); P.-G. de Gennes, *Phys. Rev.* **118**, 141 (1960).
2. R. M. Kusters, J. Siagleton, D. A. Keen, R. McGreevy, and W. Hayes, *Physica* **B155**, 362 (1989).
3. R. von Helmholt, J. Wecker, B. Holzapfel, L. Schultz, and K. Samwer, *Phys. Rev. Lett.* **71**, 2331 (1993).
4. K. Chahara, T. Ohno, M. Kasai, and Y. Kozono, *Appl. Phys. Lett.* **63**, 1990 (1993).
5. S. Jin, T. H. Tiefel, M. McCormack, R. A. Fastnacht, R. Ramesh, and L. H. Chen, *Science* **264**, 413 (1994).
6. H. L. Ju, C. Kwon, Q. Li, R. L. Greene, and T. Venkatesan, *Appl. Phys. Lett.* **65**, 2108 (1994).
7. R. Mahesh, R. Mahendiran, A. K. Raychaudhuri, and C. N. R. Rao, *J. Solid State Chem.* **114**, 297 (1995).
8. B. Raveau, A. Maignan, and V. Caignaert, *J. Solid State Chem.* **117**, 424 (1995).
9. C. N. R. Rao and A. K. Cheetham, *Science* **272**, 369 (1996).
10. J. W. Lynn, R. W. Erwin, J. A. Borchers, Q. Huang, and A. Santoro, *Phys. Rev. Lett.* **76**, 4046 (1996).
11. G. C. Xiong, Q. Li, H. L. Ju, S. M. Bhagat, S. E. Lofland, R.L. Greene, and T. Venkatesan, *Appl. Phys. Lett.* **67**, 3031 (1995).
12. *Chemical Application of Mössbauer Spectroscopy* V. I. Goldanskii and R. H. Herber (eds.), Academic Press, New York (1968).
13. Y. Takeda, S. Naka, M. Takano, T. Shinjo, T. Takada, and M. Shimada, *Mat. Res. Bull.* **13**, 61 (1978).
14. J. A. M. Van Roosmalen and E. H. P. Cordfunke, *J. Solid State Chem.* **110**, 106 (1994).
15. A. J. Millis, P. R. Littlewood, and B. I. Shraiman, *Phys. Rev. Lett.* **74**, 5144 (1995).
16. J.-H. Park, C. T. Chen, S.-W. Cheong, W. Bao, G. Meigs, V. Chakarian, and Y. U. Idzerda, *Phys. Rev. Lett.* **76**, 4215 (1996).

17. T. A. Tyson, J. Mustre de Leon, S. D. Conradson, A. R. Bishop, J. J. Neumeier, H. Röder, and J. Zang, *Phys. Rev* **B53**, 13985 (1996).
18. S. J. L. Billinge, R. G. Di Francesco, G. H. Kwei, J. J. Neumeier, and J. D. Thompson, *Phys. Rev. Lett* **77**, 715 (1996).
19. G.-M. Zhao, K. Conder, H. Keller, and K. A. Müller, *Nature* **381**, 676 (1996).
20. A. J. Millis, B. I. Shraiman, and R. Mueller, *Phys. Rev. Lett.* **77**, 175 (1996).
21. M. R. Ibarra, P. A. Algarabel, C. Marquina, J. Blasco, and J. Garcia, *Phys. Rev. Lett.* **75**, 3541 (1995).
22. P. G. Radaelli, D. E. Cox, M. Marezio, S.-W. Cheong, P. E. Schiffer, and A. P. Ramirez, *Phys. Rev. Lett.* **75**, 4488 (1995).
23. V. Caignaert, E. Suard, A. Maignan, C. Simon, and B. Raveau, *C. R. Acad. Sci.* **321**, 515 (1995).
24. P. Dai, J. Zhang, H. A. Mook, S.-H. Liou, P. A. Dowben, and E. W. Plummer, *Phys. Rev.* **B54**, R3694 (1996).
25. C. H. Booth, F. Bridges, G. J. Snyder, and T. H. Geballe, *Phys. Rev.* **B54**, R15606 (1996).
26. D. N. McIlroy, J. Zhang, S.-H. Liou, and P. A. Dowben, *Phys. Lett.* **A207**, 367 (1995).
27. J. E. Nunez-Regueiro, D. Gupta, and A. M. Kadin, *J. Appl. Phys.* **79**, 5179 (1996).
28. J.-S. Zhou, W. Archibald, and J. B. Goodenough, *Nature* **381**, 770 (1996).
29. R. P. Sharma, G. C. Xiong, C. Kwon, R. Ramesh, R. L. Greene, and T. Venkatesan, *Phys. Rev.* **B 54**, 10014 (1996).